Nanoscale

Accepted Manuscript

This article can be cited before page numbers have been issued, to do this please use: Y. Yagi, T. Kozawa, K. Yoshida, A. Uehara, M. Osada and H. Abe, *Nanoscale*, 2026, DOI: 10.1039/D5NR05307B.

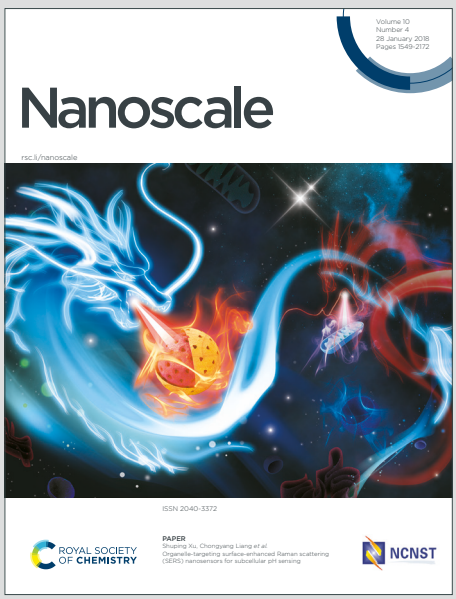

ROYAL SOCIETY OF CHEMISTRY

rsc.li/nanoscale

View Article Online
DOI: 10.1039/D5NR05307B

ARTICLE

Spontaneous Formation of Gold Nanoparticles Triggered by Hydrophobic Interfaces

Received 00th January 20xx,
Accepted 00th January 20xx

DOI: 10.1039/x0xx00000x

Yuina Yagi,[a] Takahiro Kozawa,*[b] Kanako Yoshida,[b] Akihiro Uehara,[c] Minoru Osada[d] and Hiroya Abe*[b]

Gold nanoparticles (AuNPs) underpin advances across numerous applications, yet most syntheses still rely on added chemical reductants and organic additives, constraining sustainability. Here, we report an aqueous, reductant-free route to AuNPs that leverages hydrophobic interfaces under mild conditions. When NaOH is added to aqueous $HAuCl_4$ to reach basic conditions (pH 10–13), where $[Au(OH)_4]^-$ predominates, AuNPs form spontaneously upon contact with hydrophobic fluoropolymer surfaces (e.g., PFA) without added reductants or surfactants. In contrast, almost no AuNP formation is observed on hydrophilic glass under otherwise identical conditions, indicating that interfacial rather than bulk properties govern nucleation and growth. Systematic pH tuning revealed that AuNP yield reaches a pronounced maximum at pH ≈ 12 and becomes negligible at very high alkalinity (pH 14), while particle size is tunable by varying $HAuCl_4$ and NaOH concentrations. These results, together with the suppression of AuNP formation at high ionic strength, indicate that interfacial ion distributions, rather than bulk pH alone, play a decisive role in the reaction. A consistent interpretation is that hydrophobic interfaces promote preferential adsorption of OH^-, giving rise to an electric double layer (EDL) with an ion distribution distinct from the bulk. Within this nanoscale-confined environment, ultrasmall Au(III) hydroxide-like species may form and, owing to strong size effects, undergo low-temperature transformation to yield AuNPs. These results establish interfacial EDL confinement as a basis for sustainable, reductant-free nanomaterial synthesis and suggest extension of this principle to other aqueous metal systems.

Introduction

Nanoparticle synthesis demands strategies that deliver precise structural control, minimize chemical waste, and offer clear mechanistic understanding—requirements central to advancing sustainable nanochemistry. Gold nanoparticles (AuNPs) have long served as a model platform owing to their broad applications in sensing,[1,2] catalysis,[3–5] and biomedicine.[6,7] Yet, most established protocols—dating back to Faraday's 1857 liquid-phase reduction—depend on strong chemical reductants and organic additives, complicating surface chemistry and raising sustainability concerns.[8–11] "Green" approaches employing biological reductants reduce reagent toxicity but introduce compositional variability, limited reproducibility, and additional purification steps.[12–15]

Attempts to eliminate added reductants have focused on physical methods such as laser ablation,[16–18] ultrasonic irradiation,[19,20] and radiation,[21] which require specialized instrumentation and offer limited scalability. These constraints motivate the search for approaches that exploit inherent chemical driving forces, requiring only mild thermal energy input. Interfaces offer a compelling route: unlike bulk aqueous solutions, interfacial regions exhibit localized gradients in solute concentration, pH, and electrostatics that can enable unconventional reaction pathways.[22–26] Reductant-free formation of AuNPs or gold nanoclusters has indeed been observed at microdroplet surfaces[27,28] and in confined protein nanospaces,[29] though the relative contributions of spatial confinement and interfacial effects remain unclear; moreover, microdroplet systems offer inherently low throughput.

This leads to a central question in interfacial chemistry: can interfacial driving forces, without relying on spatial confinement, be translated into macroscopic settings to enable practical reductant-free synthesis? Hydrophobic interfaces, which share key physicochemical attributes with microdroplet surfaces,[30,31] represent an attractive yet largely unexplored option. This gap exists in part because reaction vessels are rarely treated as synthetic variables, and the surface chemistry of common labware has received little attention.[32,33]

Here, we demonstrate that hydrophobic polymer interfaces, including perfluoroalkoxy alkane (PFA) and polypropylene, trigger the spontaneous formation of AuNPs from basic $HAuCl_4$ solutions (pH 10–13, adjusted with NaOH) at 25–100 °C without added reductants or surfactants, whereas hydrophilic glass remains inactive under otherwise identical conditions. Under these basic conditions, Au(III) exists predominantly as $[Au(OH)_4]^-$. The AuNP yield peaks at pH ≈ 12 and becomes

[a] Graduate School of Engineering, The University of Osaka, Osaka 565-0871, Japan.
[b] Joining and Welding Research Institute, The University of Osaka, Osaka 567-0047, Japan.
E-mail: kozawa.takahiro.jwri@osaka-u.ac.jp; abe.hiroya.jwri@osaka-u.ac.jp
[c] Institute for Radiological Science, National Institutes for Quantum Science and Technology, Chiba 263-8555, Japan.
[d] Department of Materials Chemistry & Institute of Materials and Systems for Sustainability (IMaSS), Nagoya University, Aichi 464-8601, Japan.

negligible at pH 14, revealing a clear optimum within the basic regime.

We suggest a low-temperature, thermally assisted mechanism mediated by the electric double layer (EDL), in which $[Au(OH)_4]^-$ may be locally transformed via Au(III) hydroxide-like intermediates within a nanoscale-confined interfacial environment, eventually leading to the formation of AuNPs, as elaborated in the Discussion. Collectively, these findings provide a conceptual framework for reductant-free nanomaterial synthesis and suggest that common labware surfaces may serve as an accessible platform for sustainable nanochemistry.

Methods

Materials and Reaction Vessels

Hydrogen tetrachloroaurate(III) tetrahydrate ($HAuCl_4 \cdot 4H_2O$, 99% purity) and gold(III) hydroxide ($Au(OH)_3$, ≥ 79% Au) were purchased from Kishida Chemical and Thermo Scientific, respectively. Ultrapure water (resistivity, 18.2 MΩ·cm, total organic content, < 4 ppb), NaOH solution, ammonia solution (NH_3, 28%), hydrogen peroxide (H_2O_2, 30%), concentrated hydrochloric acid (HCl), and concentrated nitric acid (HNO_3) were purchased from FUJIFILM Wako Pure Chemicals (Guaranteed Reagent). High-purity water was purchased from Sanei Chemicals. All the reagents were used without further purification. Three types of reaction vessels were used: a hydrophobic fluoropolymer vessel (perfluoroalkoxy alkane, PFA; inner volume of 60 mL, Savillex), polypropylene vessel (PP; 50 mL, Corning), and a hydrophilic glass vessel (glass test tubes, 50 mL, Maruemu).

Vessel Cleaning

PFA vessels reused in experiments were precleaned using a three-step protocol: aqua regia cleaning to dissolve residual AuNPs, NaOH rinsing to neutralize and remove oxidizing chlorine species (Cl_2/NOCl), and a Standard Clean 1 (SC-1) method to eliminate particulates and organic residues. First, vessels were filled with aqua regia (HCl/HNO_3 = 3:1) for 1 min, followed by thorough rinsing with running water for 5 min. Second, because aqua regia can leave residual oxidizing chlorine species in PFA,[34,35] a decontamination step was performed by filling the vessels with 1 M NaOH and heating at 80 °C for 3 h in an oven. After cooling, the NaOH solution was discarded, and the vessels were rinsed again with running water for 5 min. Third, the vessels were cleaned using the SC-1 method,[36] a commonly employed semiconductor processing procedure. A cleaning solution of NH_3, H_2O_2, and purified water (1:1:5 by volume) was heated to 80 °C in a water bath, and the vessels were soaked for 20 min. The solution was then discarded, and the vessels were rinsed three times with purified water, sonicated for 5 min, and dried at 100 °C for 20 min, then cooled to room temperature. For hydrophilic glass vessels, new (unused) vessels were used and only the SC-1 cleaning procedure was applied, as AuNP formation was not observed under the conditions described below.

Synthesis of AuNPs Using $HAuCl_4$ as the Precursor

View Article Online DOI: 10.1039/D5NR05707B

A 1 mM aqueous solution of $HAuCl_4$ was prepared by diluting a 100 mM stock solution of $HAuCl_4 \cdot 4H_2O$ with ultrapure water. Subsequently, 10 mL of the precursor solution and 40 mL of 10 mM NaOH (for pH adjustment) were added directly into a pre-cleaned reaction vessel. Thus, the final concentration of $HAuCl_4$ in the reaction mixture was 0.2 mM. The vessel was tightly sealed, and the mixture was agitated at 100 rpm for 24 h in a laboratory shaker (NR-30, TAITEC). The vessel was then heated at 80 °C in an oven for 20 h, followed by gradual cooling to room temperature. To investigate the effects of pH, temperature, and reaction time on the synthesis of AuNPs, a series of experiments was conducted under various conditions. The pH was adjusted from 1 to 12 using 100 mM HCl or 0–10 mM NaOH. Reaction temperatures ranged from 60 to 100 °C, and heating durations varied from 5 to 80 h.

Synthesis of AuNPs Using $Au(OH)_3$ as the Precursor

For the chloride-free synthesis, 5 mg of $Au(OH)_3$ powder was suspended in 50 mL of 10 mM NaOH and transferred into either a cleaned PFA vessel or a glass vessel. The suspensions were agitated at 100 rpm for 24 h, then heated at 80 °C for 20 h, followed by gradual cooling to room temperature.

Characterization

UV–vis absorption spectra were recorded using a spectrophotometer (V-760, JASCO) with a quartz cuvette (10×10×45 mm, Tokyo Glass Kikai). Spectra were acquired over the range of 250–800 nm using ultrapure water as the baseline. All measurements were conducted at 25 °C. The following spectral indicators were used for data analysis: the localized surface plasmon resonance (LSPR) peak wavelength (λ_{spr}) reflects particle size, with shorter wavelengths typically associated with smaller AuNPs; the absorbance at 400 nm (A_{400}) serves as an indicator of synthesis yield; and the ratio of the SPR peak absorbance to A_{450} (A_{spr}/A_{450}) provides an estimate of particle size.[37,38] Transmission electron microscopy (TEM) images were acquired using a JEM-2100 microscope (JEOL). Samples were collected via centrifugation, washed with purified water, redispersed in ethanol, and deposited onto copper grids for imaging. Particle size analysis was performed using ImageJ software (ver. 1.54g) by measuring the diameters of 458 NPs. X-ray diffraction (XRD) patterns were recorded using a diffractometer (D2 Phaser, Bruker) equipped with a Ni filter over a 2ϑ range of 30°–80°. The samples were centrifuged, washed with purified water, deposited onto a low-background silicon holder, and dried under vacuum. Phase identification was performed using the reference data for metallic gold (ICDD PDF No. 00-004-0784). Because no reference data were available for $Au(OH)_3$, a sample of $Au(OH)_3$ powder was measured under identical conditions for comparison. The concentrations of the unreacted Au complexes were determined using an energy-dispersive X-ray fluorescence (XRF) spectrometer (EDX-7000, Shimadzu). For each sample, the XRF signal was measured three times. The average value was used to calculate the AuNP yield relative to the initial precursor concentration. Potential measurements were conducted with

View Article Online
DOI: 10.1039/D5NR05307B

an ELSZ-2000 apparatus (Otsuka Electronics) at 20 °C using the Smoluchowski equation. X-ray absorption near-edge structure (XANES) measurements at the Au L3-edge were performed at beamline BL14B1 at SPring-8 (Japan). Au foil and $NaAuCl_4$ were used for energy calibration. Solid samples were analyzed in transmission mode by pressing powders onto a Scotch tape affixed to an acrylic plate. Liquid samples were measured in fluorescence mode using acrylic cells sealed with Kapton tape positioned at 90° to the detector. Data were processed with Athena software (ver. 0.9.26) from the Demeter package.

Validation of PFA Surface Cleanliness and Reductant-Free Conditions

To examine residual organic species and changes in functional groups on the PFA surface following the three-step cleaning protocol, attenuated total reflectance (ATR) Fourier-transform infrared spectroscopy (FTIR, IRSpirit, Shimadzu) measurements were performed using PFA substrates. To assess residual chloride ions after aqua regia cleaning and subsequent NaOH rinsing, and residual H_2O_2 after SC-1 cleaning, $AgNO_3$-induced AgCl precipitation and an iodine assay with UV–vis spectroscopy were employed, respectively. To assess residual chloride ions, purified water was added to the cleaned vessel and gently agitated; the resulting solution was then mixed with 1 M $AgNO_3$ aqueous solution, and the formation of insoluble AgCl precipitate was evaluated. To assess residual H_2O_2, the rinse water collected after vessel agitation was acidified with H_2SO_4, treated with 200 mM KI aqueous solution, and analyzed by UV–vis spectroscopy. Furthermore, to investigate whether radical species were generated at the PFA surface during the reaction, electron spin resonance (ESR, JES-FA-100, JEOL) analysis was performed using 5,5-dimethyl-1-pyrroline-*N*-oxide (DMPO) as a spin-trapping agent. AuNP synthesis was carried out under the standard conditions described above using PFA vessels, and the resulting solution was analyzed by ESR (Supplementary Information).

Results

Reductant-Free Synthesis of AuNPs Using a Hydrophobic Vessel

AuNPs were synthesized without added chemical reductants by heating a pH-controlled aqueous solution of the gold precursor in hydrophobic vessels (Fig. 1a). Specifically, an aqueous solution of $HAuCl_4$ adjusted to pH 12 with NaOH was transferred into hydrophobic PFA vessels whose inner surfaces had been thoroughly cleaned by sequential aqua regia, NaOH, and SC-1 treatments, and heated at 80 °C for 20 h. Following this treatment, the solution turned red (Fig. 1b), and UV–vis spectroscopy revealed a characteristic absorption band near 540 nm, corresponding to the LSPR of AuNPs (Fig. 1c). In contrast, no color change or LSPR band was observed when the reaction was carried out in hydrophilic glass vessels, suggesting that almost no reduction of Au(III) occurred and that AuNP formation was largely absent under these conditions (Fig. 1c). These findings highlight the critical role of the vessel surface in AuNP formation.

The products were obtained as colloidal solutions. Low-magnification TEM revealed that the AuNPs were relatively uniform in size and remained well-dispersed even in the absence of surfactants (Fig. 1d). High-resolution TEM further revealed the presence of polyhedral AuNPs with distinct

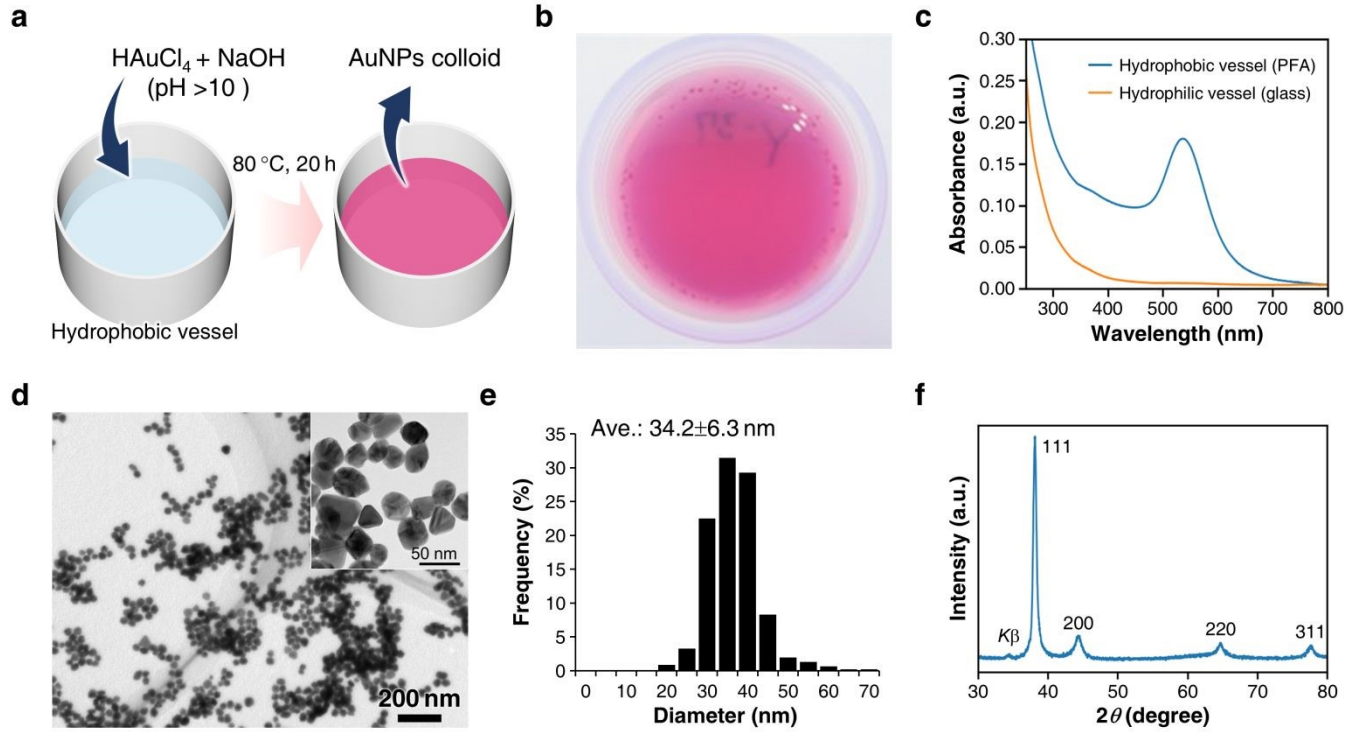

Fig. 1 Reductant-free synthesis of AuNPs in a hydrophobic PFA vessel. (a) Schematic of the synthesis procedure. (b) Photograph of the resulting colloidal solution. (c) UV–vis spectra of solutions after reaction in hydrophobic and hydrophilic vessels. (d) TEM images of the resulting colloidal particles. (e) Particle size distribution obtained from TEM image analysis. (f) XRD pattern of the dried colloidal particles.

View Article Online
DOI: 10.1039/D5NR05307B

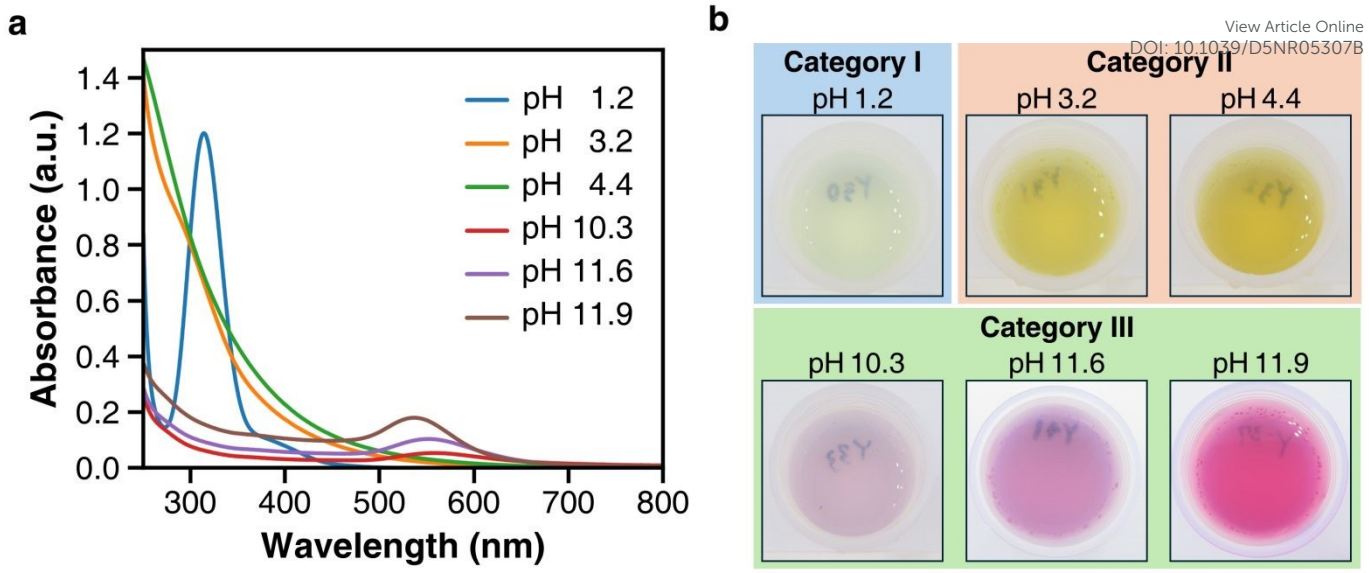

Fig. 2 pH-dependent synthesis of AuNPs in hydrophobic PFA vessels. (a) UV–vis spectra of solutions at different pH values after reaction. (b) Photographs of the resulting solutions at each pH value.

triangular facets (Fig. 1d, inset). The measured lattice spacing of 0.238 nm corresponds to the (111) plane of face-centered cubic (fcc) Au (Supplementary Fig. 1a), and the selected area electron diffraction pattern confirmed the fcc crystal structure (Supplementary Fig. 1b). The average particle size was 34.2±6.3 nm, with a coefficient of variation of 18.5% (Fig. 1e). To confirm the metallic nature of the NPs, powder XRD was performed on centrifuged and dried samples. The resulting XRD pattern exhibited Bragg reflections corresponding to the (111), (200), (220), and (311) planes of fcc Au, confirming the formation of crystalline metallic AuNPs (Fig. 1f).

XRF analysis indicated a yield of approximately 28% relative to the initial gold precursor. Zeta potential measurements yielded a value of −15 mV, suggesting colloidal stability in water without surfactants, attributable to electrostatic repulsion from negatively charged particle surfaces. Colloidal stability was maintained for several days, with signs of aggregation appearing after 5 days (Supplementary Fig. 2).

Reproducibility under standard conditions (pH 12, 80 °C, 20 h, PFA vessel) was evaluated across 27 independent syntheses. The λ_{spr} values ranged from 531 to 553 nm (average: 540 nm), and the average A_{400} and A_{spr}/A_{450} values were 0.09±0.01 and 1.88±0.06, respectively (Supplementary Fig. 3). These results demonstrate the high reproducibility of the optical properties, yields, and particle size of the synthesized AuNPs.

Influence of Solution pH

AuNP formation was highly dependent on the pH of the reaction medium. To investigate this parameter systematically, AuNP formation was examined in hydrophobic PFA vessels over a range of pH conditions. UV–vis spectra and corresponding photographs of the resulting solutions are shown in Fig. 2, and the outcomes were classified into three categories.

(I) Strongly acidic conditions (pH ≈ 1): In solutions adjusted to pH ≈ 1 with 100 mM HCl, no visible changes were observed after heating. The solution retained its pale-yellow color with no Tyndall effect (Supplementary Fig. 4), indicating the absence of NP formation. The UV–vis spectrum exhibited a strong absorption band at 314 nm, characteristic of dissolved $[AuCl_4]^-$.[39]

(II) Weakly acidic conditions (pH 3–5): In solutions adjusted to pH 3–5 with 0–1 mM NaOH, the color intensified to a deeper yellow and a clear Tyndall effect was observed (Supplementary Fig. 4), suggesting the formation of dispersed particulate species. The UV–vis spectra showed broad absorption below 450 nm without distinct plasmonic bands. XRD analysis of the precipitate obtained at pH 4.4 revealed diffraction patterns consistent with $Au(OH)_3$ (Supplementary Fig. 5), indicating that $Au(OH)_3$ was the predominant product under these conditions. The precipitated $Au(OH)_3$ particles were spherical with an average diameter of approximately 22 nm.

(III) Basic conditions (pH > 10): In solutions adjusted to pH > 10 with 2–10 mM NaOH, the solution turned red upon heating and a distinct Tyndall effect was observed (Supplementary Fig. 4), confirming NP formation. The UV–vis spectra exhibited well-defined LSPR peaks in the 536–558 nm range. Within this basic regime, however, AuNP formation exhibited a clear optimum with respect to NaOH concentration rather than a monotonic increase. At pH 10–12, the A_{400} value increased from 0.03 to 0.09 with increasing pH, confirming an improvement in synthesis yield, while the A_{spr}/A_{450} ratio decreased from 2.04 to 1.88, suggesting the formation of smaller AuNPs. Beyond this optimum, the yield decreased markedly: at pH 12.7, A_{400} fell to 0.01, with only significantly smaller particles (5.4±2.4 nm by TEM) detected (Supplementary Fig. 6). At pH 14, the solution remained colorless and transparent, and AuNP formation was almost suppressed (Supplementary Fig. 7). These results demonstrate that AuNP formation within the basic regime is non-monotonic, with an optimum around pH 12 and near-complete suppression at pH 14.

Notably, the pH remained nearly unchanged before and after the reaction under both strongly acidic (Category I) and

View Article Online
DOI: 10.1039/D5NR05307B

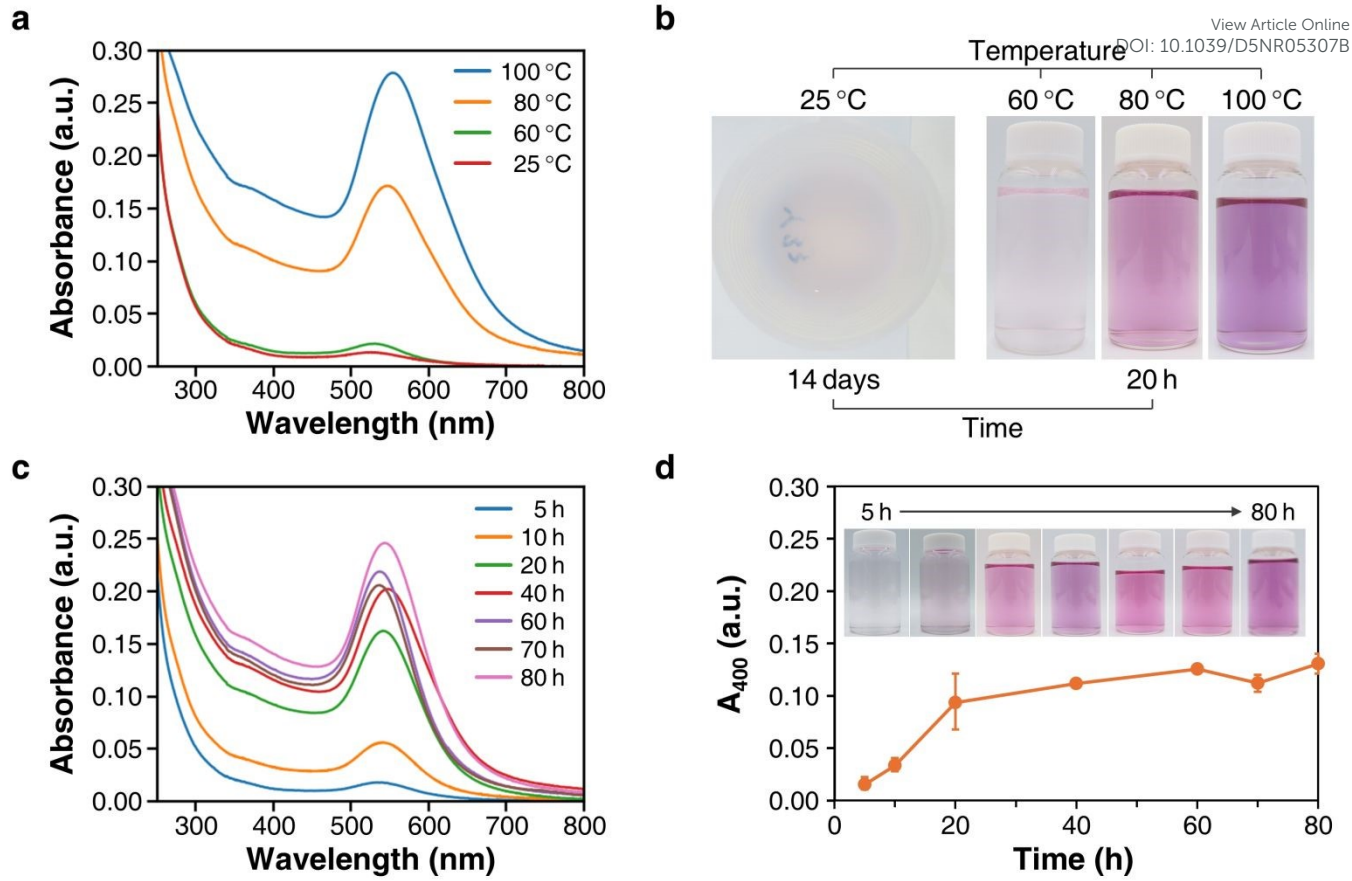

Fig. 3 Effects of temperature and reaction time on AuNP formation in hydrophobic PFA vessels. (a) UV–vis spectra of solutions after reaction at different temperatures. (b) Photographs of colloidal solutions obtained at different temperatures. (c) Time-dependent UV–vis spectra of solutions reacted at 80 °C. (d) Time course of A_{400} for solutions reacted at 80 °C (n = 5, 5–10 h; n = 27, 20 h; n = 2, ≥ 40 h).

basic (Category III) conditions. In contrast, under weakly acidic conditions (Category II), the pH decreased from 5.7 to 4.4 upon heating at 80 °C (Supplementary Table 1), indicating proton generation during the hydrolysis of Au(III) and subsequent precipitation of $Au(OH)_3$.

Influence of Reaction Temperature, Time, and $HAuCl_4$ Concentration

Having established the critical role of basic pH, we next systematically examined how temperature, reaction time, and $HAuCl_4$ concentration influence AuNP formation in hydrophobic PFA vessels (Supplementary Table 2). We first investigated the effects of temperature and reaction time. UV–vis spectra recorded after 20 h of heating showed that A_{400} increased from 0.01 to 0.12 with increasing temperature up to 100 °C (Fig. 3a). Although A_{spr} was nearly negligible at 25 °C, a plasmonic band emerged at 60 °C and intensified sharply above 80 °C. The solution heated to 60 °C developed a slight red coloration, whereas at 25 °C only a faint color change appeared after 14 days of storage (Fig. 3b). Additionally, λ_{spr} shifted from 530 nm at 60 °C to 553 nm at 100 °C, suggesting an increase in particle size with temperature (Fig. 3a), consistent with the corresponding increase in A_{spr}/A_{450} from 1.72 to 1.93 over the same temperature range.

The time-dependent behavior was examined at 80 °C to assess the growth dynamics and yield of AuNPs. A_{400} increased with reaction time and reached a plateau after 20 h, indicating saturation of NP formation (Figs. 3c and 3d). Throughout the reaction, λ_{spr} remained constant, and the A_{spr}/A_{450} ratio showed little variation from 5 to 80 h (Supplementary Table 2), indicating that particle size was established early while the number of particles continued to increase over time.

Next, the effect of initial $HAuCl_4$ concentration on AuNP formation was investigated by varying the concentration from 0.2 to 5 mM (corresponding to final concentrations of 0.04–1 mM at pH 12). At the lowest concentration of 0.2 mM, TEM analysis revealed an average particle size of 57.9±9.0 nm (Supplementary Fig. 8), larger than that obtained under the standard conditions (34.2 nm; Fig. 1e). A_{spr}/A_{450} decreased monotonically from 1.93 to 1.64 with increasing $HAuCl_4$ concentration, suggesting a decrease in particle size, while A_{400} remained nearly constant except at the lowest concentration of 0.2 mM (Supplementary Table 2). Taken together with the temperature and reaction time dependences described above, these results indicate that temperature and reaction time are the primary factors governing yield, whereas NaOH and $HAuCl_4$ concentrations are the primary factors controlling particle size.

Attempts at AuNP Synthesis Using a Hydrophilic Glass Vessel

View Article Online
DOI: 10.1039/D5NR05307B

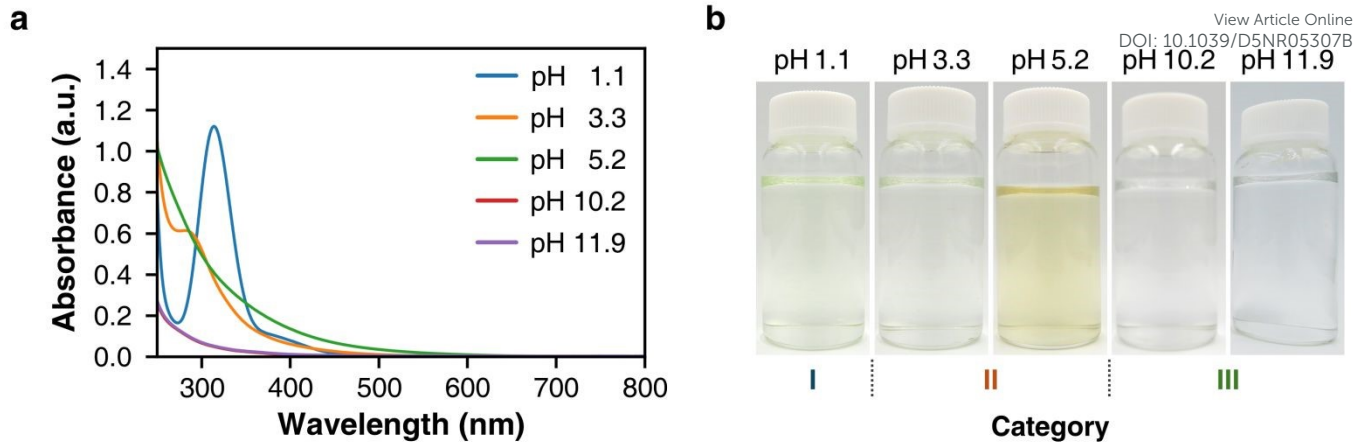

Fig. 4 pH-dependent AuNP formation in hydrophilic glass vessels. (a) UV–vis spectra of solutions at different pH values after reaction. (b) Photographs of the resulting solutions at each pH value.

To further clarify the influence of vessel surface chemistry, comparative experiments were conducted using hydrophilic glass vessels (Fig. 4). The results were classified into three categories analogous to those observed in the hydrophobic PFA vessels. *Category I (pH ≈ 1)*: Under strongly acidic conditions, the solution remained pale yellow after heating, consistent with the behavior in PFA vessels. The UV–vis spectrum exhibited an absorption band characteristic of $[AuCl_4]^-$, indicating no NP formation. *Category II (pH 3–5)*: The solution developed a deeper yellow color and the Tyndall effect was observed (data not shown), suggesting the presence of dispersed particulate species. However, no plasmonic bands appeared in the UV–vis spectra, indicating that $Au(OH)_3$ was the predominant product. *Category III (pH > 10)*: In sharp contrast to the results in hydrophobic vessels, the solutions remained colorless and transparent after heating, with no LSPR peaks detected. These results indicate that almost no AuNP formation occurred in hydrophilic vessels, even under conditions that promoted NP synthesis in hydrophobic vessels. Notably, the pH remained essentially unchanged before and after the reaction in Categories I and III. In Category II with 1 mM NaOH, the pH decreased from 6.9 to 5.2, consistent with the trend observed in PFA vessels (Supplementary Table 1).

Cleanliness of Hydrophobic Interfaces

Since hydrophobic interfaces play a crucial role in reductant-free AuNP synthesis, the cleanliness of the vessel surface in contact with the solution is essential for ensuring reproducible NP formation. To this end, the effects of vessel cleaning protocols on AuNP formation were systematically examined.

The cleanliness of PFA vessels significantly impacted the reproducibility of AuNP formation (Supplementary Fig. 9). Without cleaning, A_{400} remained below 0.06, and almost no AuNPs were formed. When vessels were cleaned solely by the SC-1 method to remove surface contaminants and organic residues, substantial variations were observed in both λ_{spr} and A_{spr}. Even after removing the residual AuNPs with aqua regia, followed by SC-1 cleaning, AuNP formation remained minimal, likely due to residual oxidizing chlorine species (Cl_2/NOCl) adsorbed on the PFA surface after aqua regia treatment, which inhibit NP formation.[34] To address this, a heated NaOH rinse was introduced after aqua regia cleaning to eliminate these species, followed by SC-1 cleaning. To verify the effectiveness of this protocol, $AgNO_3$-induced AgCl precipitation tests and FTIR measurements were performed before and after each cleaning step. The absence of AgCl formation after the NaOH rinse indicated effective removal of chlorine species (Supplementary Fig. 10), and FTIR spectra showed no detectable changes in the PFA skeletal structure, while revealing a significant decrease in surface-adsorbed organic residues after SC-1 cleaning (Supplementary Fig. 11). Importantly, the cleaned PFA vessels exhibited no detectable redox activity: UV–vis analysis using the iodine assay revealed the absence of residual H_2O_2 after SC-1 cleaning (Supplementary Fig. 12). Thus, within the sensitivity of these measurements, the cleaning protocol does not chemically modify or activate the PFA surface but rather restores a clean hydrophobic surface by removing species that would otherwise inhibit AuNP formation.

Static water contact angle measurements[40] indicated that the PFA surface retains a comparable hydrophobic character after the cleaning protocol. A value of 106.8±1.8° was obtained after the full cleaning protocol, which is in reasonable agreement with the reported contact angle of fluoropolymer surfaces (≈115°),[41] with any minor deviation attributable to known variations in surface condition and processing history. Combined with the FTIR results showing no detectable formation of hydrophilic functional groups, these measurements reveal that the cleaning protocol removes surface contaminants without modifying the PFA interface at either the microscopic or macroscopic level.

By implementing this three-step cleaning protocol—comprising aqua regia treatment, heated NaOH rinsing, and SC-1 cleaning—a higher average A_{400} and reduced variation in both λ_{spr} and A_{400} were achieved (Supplementary Fig. 9). These results underscore the importance of surface cleanliness for consistent and efficient AuNP synthesis at hydrophobic interfaces.

View Article Online
DOI: 10.1039/D5NR05307B

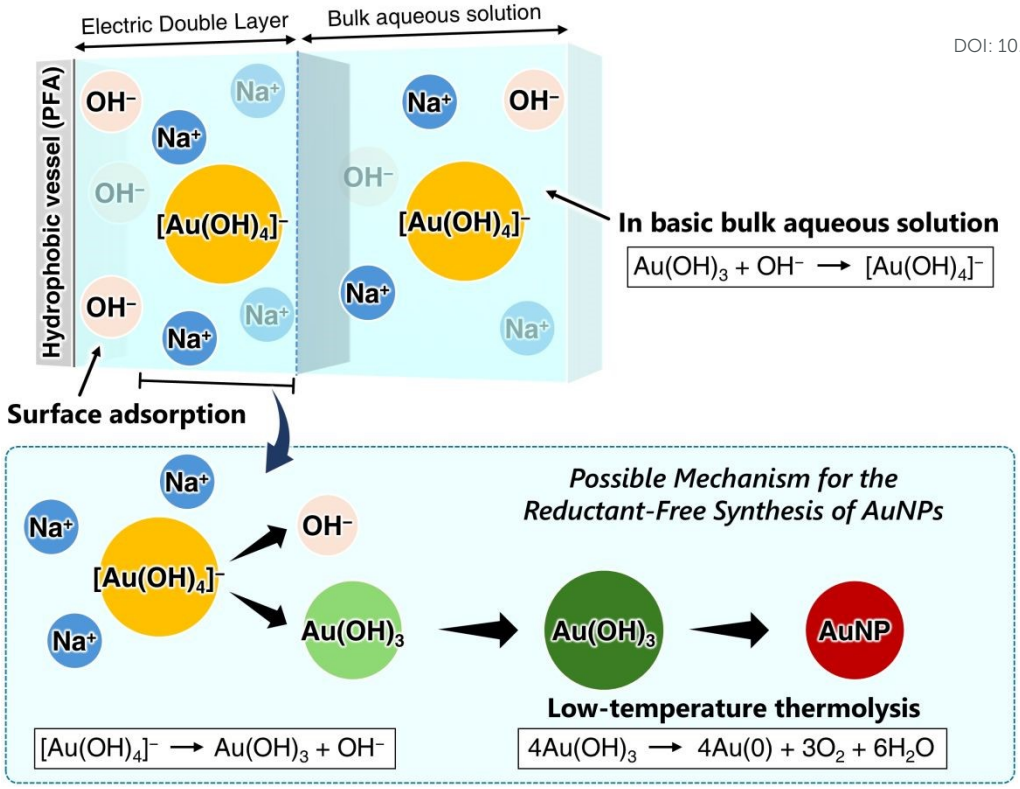

Fig. 5 Schematic illustration of a mechanistic interpretation for reductant-free AuNP formation under basic conditions at hydrophobic interfaces.

Discussion

Hydrophobic interfaces are essential for reductant-free AuNP formation: AuNPs formed reproducibly in hydrophobic PFA vessels heated under basic conditions (pH > 10), whereas almost no particles were detected in hydrophilic glass under identical conditions. This contrast demonstrates that interfacial rather than bulk properties are decisive and that the solid–liquid interface actively governs nucleation and growth.

Au(III) Complex Ion for Reductant-Free AuNP Formation

Under basic conditions (Category III), chloride-to-hydroxide ligand exchange yields $[Au(OH)_4]^-$ as the predominant Au(III) species (Supplementary Fig. 13). Although $[Au(OH)_4]^-$ is kinetically persistent in bulk solution,[39] it is not inert near hydrophobic interfaces, where conversion to metallic Au is observed upon heating.

XANES analysis revealed $[Au(OH)_4]^-$ as the sole Au(III) species prior to heating. Upon thermal treatment in PFA vessels, a fraction converted to metallic Au (Supplementary Fig. 14). Parallel experiments using commercial $Au(OH)_3$ were also performed. Although $Au(OH)_3$ is poorly soluble in water, it dissolves in 10 mM NaOH (pH 12) owing to its amphoteric nature to regenerate $[Au(OH)_4]^-$ (Eq. 1).[42] Under these conditions, AuNPs formed exclusively in PFA, not in glass (Supplementary Fig. 15). Together, these results confirm that both $[Au(OH)_4]^-$ and a hydrophobic interface are required.

$$Au(OH)_3 + OH^- \rightarrow [Au(OH)_4]^- \quad (1)$$

Assessing Alternative Reductive Pathways

To examine alternative reductive pathways, we performed three control experiments. FTIR spectra before and after the cleaning protocol revealed no detectable chemical modification of PFA (Supplementary Fig. 11). The iodine assay detected no residual H_2O_2 (Supplementary Fig. 12). Furthermore, ESR measurements using the DMPO spin-trapping agent detected no radical species generated in PFA vessels (Supplementary Fig. 16). These results suggest that the H_2O_2-mediated radical mechanism reported for sonicated fluoropolymer systems[43–45] is not operative under our conditions. Collectively, these controls indicate that exogenous reductants, substrate-derived radicals, and residual H_2O_2 are not detectable under our conditions, arguing against these alternative reductive pathways.

Mechanistic Interpretation: EDL-Mediated Interfacial Thermolysis

We present that AuNP formation in this system is an interface-specific process governed by the composition and effective thickness of the EDL that forms spontaneously at hydrophobic surfaces. Three lines of experimental evidence support this view.

(i) Zeta potential measurements at pH ≈ 10 (Supplementary Table 3) yield comparable values for PFA (−83.4±4.2 mV) and glass (−71.4±1.1 mV), yet only the hydrophobic surface supports AuNP formation. This indicates that interfacial field strength alone does not determine reactivity; rather, the origin of surface charging and the resulting EDL composition are the decisive factors.

View Article Online DOI: 10.1039/D5NR05707B

(ii) The AuNP yield (A_{400}) increases from pH 10 to pH 12 but drops sharply at pH 12.7, exhibiting a pronounced maximum (Supplementary Fig. 6, Table 2). At pH 14 (1 M NaOH), the Debye length (λ_D) shrinks to approximately 0.3 nm (Supplementary Table 4), almost suppressing AuNP formation. Thus, the yield rises and then collapses as the EDL is progressively compressed, indicating that nucleation is optimized at an intermediate EDL thickness but suppressed when the diffuse layer becomes over-compressed at very high alkalinity. This behavior provides a direct experimental signature of EDL-controlled nucleation that bulk Au(III) speciation alone cannot explain.

(iii) Further support comes from ionic-strength control experiments: addition of 1 M NaCl to the pH 12 reaction medium—while maintaining pH and with Au(III) remaining predominantly as $[Au(OH)_4]^-$ (Supplementary Fig. 17)—almost suppressed AuNP formation (Supplementary Fig. 18), mirroring the effect observed at pH 14 (1 M NaOH). Because NaCl compresses the EDL independently of pH and Au(III) speciation ($\lambda_D \approx 0.3$ nm; Supplementary Table 4), this result provides direct evidence that EDL thickness, rather than pH per se, is the critical variable governing reactivity, isolating EDL compression as the dominant factor.

Building on (i)–(iii), we outline a mechanistic interpretation in which the diffuse layer at hydrophobic interfaces serves as the reaction environment (Fig. 5), consistent with controls indicating that external reductants, substrate-derived radicals, and residual H_2O_2 are below detectable levels (Supplementary Figs. 11, 12, 16).

The key factor distinguishing PFA from glass lies in the origin of surface charge and the resulting EDL composition. At hydrophobic PFA, the interfacial potential is dominated by specific adsorption of OH^- in the Stern layer,[46] which creates an OH^--enriched Stern layer and a correspondingly OH^--depleted diffuse layer, as schematically summarized in Fig. 5. In contrast, at hydrophilic glass, the negative surface charge originates from silanol deprotonation,[47,48] and OH^- is not specifically adsorbed (Supplementary Fig. 19). Consequently, near-interface ion partitioning differs fundamentally, and the local OH^- depletion required to promote $Au(OH)_3$-like nucleation is unlikely to establish at glass.

At hydrophobic interfaces, the local OH^- activity adjacent to the PFA surface is lower than in bulk solution due to EDL partitioning, shifting the following equilibrium toward $Au(OH)_3$-like species within the interfacial zone (Fig. 5):

$$[Au(OH)_4]^- \leftrightarrow Au(OH)_3 + OH^- \quad (2)$$

$Au(OH)_3$ is sparingly soluble in water yet amphoteric; therefore, $Au(OH)_3$-like species that escape into bulk alkaline solution are expected to rapidly redissolve to $[Au(OH)_4]^-$, explaining why such intermediates remain spatially localized at the interface and do not accumulate as bulk-detectable species.

Such interfacial $Au(OH)_3$-like species are expected to be ultrasmall, as their dimensions are constrained by the nanoscale EDL region. Due to strong size effects, ultrasmall species exhibit thermodynamic and kinetic properties distinct from bulk $Au(OH)_3$, whose decomposition to Au(0) proceeds via Au_2O_3 and requires approximately 300 °C in air.[49] Surface-energy contributions become dominant at reduced dimensions, lowering the activation barrier for the following transformation:

$$4Au(OH)_3 \rightarrow 4Au(0) + 3O_2 + 6H_2O \quad (3)$$

To directly assess this size-dependent transformation, colloidal $Au(OH)_3$ nanoparticles (average diameter: 22 nm) prepared under Category II conditions (Supplementary Fig. 5) were subjected to hydrothermal treatment at 140 °C for 10 h. XRD confirmed metallic Au peaks alongside residual amorphous $Au(OH)_3$, and TEM revealed irregularly shaped AuNPs coexisting with unreacted spherical $Au(OH)_3$ particles (Supplementary Fig. 20), demonstrating partial transformation at temperatures far below those required for bulk decomposition. The coexistence of AuNPs and $Au(OH)_3$ phases likely reflects a broad particle-size distribution and local heterogeneity. Nevertheless, the key conclusion—that small $Au(OH)_3$ species can undergo low-temperature transformation to Au(0) without external reductants—is strongly supported. Since the $Au(OH)_3$-like species confined within the EDL are expected to be considerably smaller than the 22 nm Category II particles, thermolysis at relatively mild temperatures (e.g., 80 °C) becomes thermodynamically and kinetically accessible.

The most reasonable interpretation is therefore that Au(0) formation originates from the thermal transformation of interfacial Au(III) hydroxide species rather than external reductants—an interpretation that consistently accounts for the dependence on vessel material (PFA vs. glass) and ionic strength, indicating that AuNP formation is governed by a localized interfacial reaction environment rather than a homogeneous bulk-solution process. Several aspects remain unresolved, including the detailed mechanism of OH^- specific adsorption, the time-dependent ion distributions within the EDL, and the nucleation and growth dynamics of interfacial $Au(OH)_3$-like species; direct observation of such transient species in nanoscale-confined environments remains an important future challenge.

Within the parameter ranges examined here ($HAuCl_4$ = 0.2–5 mM, NaOH = 2–50 mM), particle size can be modulated by both NaOH and $HAuCl_4$ concentrations, albeit via distinct mechanisms. Increasing NaOH from pH 10 to 12 yields smaller particles, whereas increasing $HAuCl_4$ concentration also shifts the size to smaller values, though the effect is less pronounced. Reaction time predominantly influences yield with little impact on size, while temperature affects both. These trends are consistent with the EDL-mediated mechanistic interpretation: NaOH largely determines ionic strength and thus EDL thickness, so increasing NaOH compresses the diffuse layer, reduces the effective interfacial reaction volume, and elevates local supersaturation—favoring more, smaller nuclei. In contrast, varying $HAuCl_4$ has a comparatively minor effect on EDL thickness when NaOH dominates ionic strength; its influence on particle size more plausibly arises from changes in the availability of Au(III) species to the interfacial zone and the balance between nucleation and subsequent growth. Together, NaOH (EDL confinement) and $HAuCl_4$ (Au(III) supply and nucleation–growth balance) provide complementary handles for tuning particle size under reductant-free, interfacial conditions.

View Article Online
DOI: 10.1039/D5NR05307B

Overall, productive AuNP formation requires a diffuse layer that is sufficiently developed to create an environment distinct from the bulk, yet not over-compressed by excessive ionic strength—consistent with the pronounced maximum in the pH–yield profile and the suppression observed upon adding 1 M NaCl at constant pH. This framework is qualitative and intended as a guiding picture rather than a quantitative kinetic model. Notably, this pathway is mechanistically distinct from the reductant-free AuNP formation reported by Macchione et al.,[50] which occurs in homogeneous solution without surface selectivity. To provide more direct experimental evidence for the proposed mechanistic interpretation, in-situ detection of transient interfacial $Au(OH)_3$-like species, verification of O_2 evolution using a sealed reactor, and direct measurement of the existence and magnitude of the interfacial electric field remain important future challenges.

Prediction and Experimental Verification of Generality

The proposed mechanistic interpretation predicts that reductant-free AuNP formation should be enabled at hydrophobic solid–liquid interfaces supporting preferential OH^- adsorption and an interfacial EDL environment, even for chemically distinct polymers. To test this prediction, we conducted experiments using PP vessels, which are chemically unrelated to fluoropolymers but similarly hydrophobic. AuNPs also formed in PP under otherwise identical reductant-free conditions (Supplementary Fig. 21), supporting the prediction and suggesting that reductant-free AuNP formation can extend beyond fluoropolymer substrates.

Scope, Limitations, and Outlook

This approach produces surfactant-free AuNPs in water without any added reductant but currently has practical limitations: a reaction time of 20 h and a modest conversion yield (≈ 28%). These values are less favorable than conventional reductant-based protocols, which often reach higher yields on much shorter timescales.[51,52] Reproducibility is sensitive to surface cleanliness, as residual oxidizing species or gold deposits suppress nucleation. Yield improvements may be achieved by increasing the available hydrophobic interfacial area or by enhancing mass transport of $[Au(OH)_4]^-$ to the interface (e.g., by controlled convection or mixing). Nonetheless, NaOH and precursor concentrations, temperature, and reaction time provide handles for tuning particle size and yield, and the generality demonstrated across PFA and PP suggests that more environmentally benign hydrophobic substrates may serve as viable alternatives.[53] Future efforts will focus on scale-up through interfacial area enlargement, achieving precise size and morphology control, and extending the principle to other noble metal systems.

Conclusions

This study establishes a reductant-free route to AuNPs driven by hydrophobic interfaces under basic aqueous conditions. AuNPs formed reproducibly in hydrophobic PFA vessels at pH 10–13, whereas almost no particles were detected in hydrophilic glass under identical conditions, demonstrating that interfacial properties, rather than bulk solution chemistry, govern nucleation and growth.

The results support an EDL-mediated interfacial pathway in which preferential OH^- adsorption at hydrophobic surfaces produces an interfacial environment distinct from the bulk, including a reduced effective OH^- activity in the diffuse layer. This local condition can shift Au(III) chemistry from $[Au(OH)_4]^-$ toward interfacially confined $Au(OH)_3$-like species, which, owing to strong size effects, undergo low-temperature thermal transformation to metallic Au(0). The AuNP yield increases from pH 10 to 12 and decreases at higher alkalinity; at pH 14 (1 M NaOH) and upon addition of 1 M NaCl at constant pH, AuNP formation is suppressed, consistent with inhibition under EDL compression. Control experiments indicate that alternative reductive pathways involving residual H_2O_2 or hydroxyl radicals are not operative, and hydrothermal aging of colloidal $Au(OH)_3$ provides direct evidence that nanoscale gold hydroxide can partially transform to Au(0) at temperatures far below bulk decomposition.

The resulting AuNPs are surfactant-free and colloidally stable for several days, with their size and yield tunable through NaOH and precursor concentrations, temperature, and reaction time. The generality of this mechanistic interpretation across chemically distinct hydrophobic surfaces points to broad applicability in other noble metal systems and offers a conceptual framework for sustainable, interface-engineered nanomaterial synthesis.

Author contributions

H.A. conceived the project. Y.Y., T.K. and H.A. designed the experiments. Y.Y., T.K., K.Y., A.U. and M.O. performed the experiments. All authors contributed to the data analysis. Y.Y., T.K., M.O. and H.A. prepared the manuscript, and all authors contributed to manuscript revisions.

Conflicts of interest

There are no conflicts to declare.

Data availability

The data supporting the findings of this study are available within this Article and its Supplementary Information.

Acknowledgements

This work was funded by Grants-in-Aid for Scientific Research KAKENHI (24K21675, 24K01180), the Japan Society for the Promotion of Science (JSPS), and the Cooperative Research Project of Design & Engineering by Joint Inverse Innovation for Materials Architecture (DEJI²MA), MEXT. X-ray absorption measurements were performed at the beamline BL14B1, SPring-8, Japan on the proposal No. 2024B3662.

References

1 Y. Hang, A. Wang and N. Wu, *Chem. Soc. Rev.*, 2024, **53**, 2932–2971.
2 S. Palani, J. P. Kenison, S. Sabuncu, T. Huang, F. Civitci, S. Esener and X. Nan, *ACS Nano*, 2023, **17**, 2266–2278.
3 H. Sheng, J. Wang, J. Huang, Z. Li, G. Ren, L. Zhang, L. Yu, M. Zhao, X. Li, G. Li, N. Wang, C. Shen and G. Lu, *Nat. Commun.*, 2023, **14**, 1528.
4 E. S. Varo, R. E. Tankard, J. Kryger-Baggesen, J. Jinsschek, S. Helveg, I. Chorkendorff, C. D. Damsgaard and J. Kibsgaard, *J. Am. Chem. Soc.*, 2024, **146**, 2015–2023.
5 K. Xia, T. Yatabe, K. Yonesato, S. Kikkawa, S. Yamazoe, A. Nakata, R. Ishikawa, N. Shibata, Y. Ikuhara, K. Yamaguchi and K. Suzuki, *Nat. Commun.,* 2024, **15**, 851.
6 Z. R. Goddard, M. J. Marín, D. A. Russell and Mark Searcey, *Chem. Soc. Rev.*, 2020, **49**, 8774–8789.
7 N. D. Calvert, J. Baxter, A. A. Torrens, J. Thompson, A. Kirby, J. Walia, S. Ntais, E. Hemmer, P. Berini, B. Hibbert, L. Ramunno and A. J. Shuhendler, *Nat. Nanotechnol.*, 2025, **20**, 276–285.
8 M. Faraday, *Philos. Trans. R. Soc. Lond.*, 1857, **147**, 145–181.
9 J. Turkevich, P. C. Stevenson and J. Hillier, *Discuss. Faraday Soc.*, 1951, **11**, 55–75.
10 M. Brust, M. Walker, D. Bethell, D. J. Schiffrin and R. Whyman, *J. Chem. Soc., Chem. Commun.*, 1994, **7**, 801–802.
11 S. Iravani, *Green Chem.*, 2011, **13**, 2638–2650.
12 S. P. Chandran, M. Chaudhary, R. Pasricha, A. Ahmad and M. Sastry, *Biotechnol. Prog.*, 2006, **22**, 577–583.
13 T. Khan, N. Ullah, M. A. Khan, Z.-U.-R. Mashwani and A. Nadhman, *Adv. Colloid Interface Sci.*, 2019, **272**, 102017.
14 J. S. Boruah, C. Devi, U. Hazarika, P. V. B. Reddy, D. Chowdhury, M. Barthakur and P. Kalita, *RSC Adv.*, 2021, **11**, 28029–28041.
15 V. Mehra, S. Kumar, A. M. Tamang and S. K. Chandraker, *BioNanoScience*, 2025, **15**, 18.
16 V. Amendola and M. Meneghetti, *Phys. Chem. Chem. Phys.*, 2009, **11**, 3805–3821.
17 R. Riedel, N. Mahr, C. Yao, A. Wu, F. Yang and N. Hampp, *Nanoscale*, 2020, **12**, 3007–3018.
18 B. S. Hettiarachchi, Y. Takaoka, Y. Uetake, Y. Yakiyama, H. H. Lim, T. Taira, M. Maruyama, Y. Mori, H. Y. Yoshikawa and H. Sakurai, *Ind. Chem. Mater.*, 2024, **2**, 340–347.
19 C.-H. Su, P.-L. Wu and C.-S. Yeh, *J. Phys. Chem. B*, 2003, **107**, 14240–14243.
20 T. Sakai, H. Enomoto, H. Sakai and M. Abe, *Colloids Surf., A*, 2009, **347**, 18–26.
21 K. Weinel, M. B. Hahn, A. Lubk, W. Feng, I. G. G. Martinez, B. Büchner and L. A. Jácome, *ACS Appl. Nano Mater.*, 2025, **8**, 4980–4988.
22 S. Yang, M. Li, J. Wang, V. H. Grassian, S. Kumar and C. S. Dutcher, *J. Phys. Chem. A*, 2025, **129**, 6424–6436.
23 X. Yan, R. M. Bain and R. G. Cooks, *Angew. Chem. Int. Ed.*, 2016, **55**, 12960–12972.
24 Z. Wei, Y. Li, R. G. Cooks and X. Yan, *Annu. Rev. Phys. Chem.*, 2020, **71**, 31–51.
25 Z. Liu, Y. Jiang, Z. Zhang, X. Wang, K. Liu, Z. Qiao, M. Liu, S. Zhang, Z. Mu, Q. Zhang and C. Gao, *Nat. Synth.*, 2023, **2**, 119–128.
26 K. Y. Chan, C. Zhuang, V. G. Vuong, N. Qian, X. Gao and W. Min, *Chem. Soc. Rev.*, 2026, **55**, 336–357.
27 J. K. Lee, D. Samanta, H. G. Nam and R. N. Zare, *Nat. Commun.*, 2018, **9**, 1562.
28 M. A. Eatoo, N. Wehbe, N. Kharbatia, X. Guo and H. Mishra, *Chem. Sci.*, 2025, **16**, 1115–1125.
29 C. Sun, H. Yang and Y. Yuan, *J. Am. Chem. Soc.*, 2011, **133**, 8617–8624.
30 A. P. Willard and D. Chandler, *J. Chem. Phys.*, 2014, **141**, 18C519.
31 S. Strazdaite, J. Versluis and H. J. Bakker, *J. Chem. Phys.*, 2015, **143**, 084708.
32 S. Li, X. Huang, H. Li, H. Cai, C. L. Gan, F. Boey and H. Zhang, *Small*, 2010, **6**, 2708–2715.
33 M. M. Nielsen and C. M. Pedersen, *Chem. Sci.*, 2022, **13**, 6181–6196.
34 C. J. Mason, M. Edwards and P. Riby, *Analyst*, 2000, **125**, 327–332.
35 S. Recchia, D. Spanu, D. Bianchi, C. Dossi, A. Pozzi and D. Monticelli, *Talanta*, 2016, **159**, 29–33.
36 W. Kern and D. A. Puotinen, *RCA Rev.*, 1970, **31**, 187–206.
37 W. Haiss, N. T. K. Thanh, J. Aveyard and D. G. Fernig, *Anal. Chem.*, 2007, **79**, 4215–4221.
38 J. Quinson, *J. Chem. Educ.* 2023, **100**, 3612–3619.
39 A. Usher, D. C. McPhail and J. Brugger, *Geochim. Cosmochim. Acta*, 2009, **73**, 3359–3380.
40 M. Y. Alkawareek, B. M. Akkelah, S. M. Mansour, H. M. Amro, S. R. Abulateefeh and A. M. Alkilany, *J. Chem. Educ.*, 2018, **95**, 2227–2232.
41 J. N. Israelachvili, *Intermolecular and surface forces*, Academic press, 1991.
42 M. Haruta, Gold *Bull.*, 2004, **37**, 27–36.
43 J. Zhao, X. Zhang, J. Xu, W. Tang, Z. L. Wang and W. R. Fan, *Angew. Chem. Int. Ed.*, 2023, **62**, e202300604.,
44 Y. Wang, P. Wei, Z. Shen, C. Wang, J. Ding, W. Zhang, X. Jin, C. D. Vecitis and G. Gao, *Environ. Sci. Technol.*, 2024, **58**, 925–934.
45 H. Yan, X. Song, S. Li, J. Li, J. Zhang, Y. Zhang and L. Zhang, *ChemNanoMat*, 2025, **11**, e202500050.
46 L. S. McCarty and G. M. Whitesides, *Angew. Chem. Int. Ed.*, 2008, **47**, 2188–2207.
47 L. T. Zhuravlev, *Colloids Surf. A*, 2000, **173**, 1–38.
48 P. M. Dove and C. M. Craven, *Geochim. Cosmochim. Acta*, 2005, **69**, 4963–4970.
49 D. Kawamoto, H. Ando, H. Ohashi, Y. Kobayashi, T. Honma, T. Ishida, M. Tokunaga, Y. Okaue, S. Utsunomiya and T. Yokoyama, *Bull. Chem. Soc. Jpn.*, 2016, **89**, 1385–1390.
50 M. A. Macchione, J. E. Samaniego, R. Moiraghi, N. Passrelli, V. A. Macagno, E. A. Coronado, M. J. Yacaman and M. A. Pérez, *RSC Adv.*, 2018, **8**, 19979.
51 C. Deraedt, L. Salmon, S. Gatard, R. Ciganda, R. Hernandez, J. Ruiz and D. Astruc, *Chem. Commun.*, 2014, **50**, 14194–14196.
52 J. Quinson, O. Aalling-Frederiksen, W. L. Dacayan, J. D. Bjerregaard, K. D. Jensen, M. R. V. Jørgensen, I. Kantor, D. R. Sørensen, L. T. Kuhn, M. S. Johnson, M. Escudero-Escribano, S. B. Simonsen and K. M. Ø. Jensen, *Chem. Mater.*, 2023, **35**, 2173–2190.
53 J. Quinson, *Langmuir*, 2025, **41**, 33669–33676.

View Article Online
DOI: 10.1039/D5NR05307B

Data Availability Statement

View Article Online
DOI: 10.1039/D5NR05307B

The data supporting the findings of this study are available within this Article and its Supplementary Information.